# Multimaterial Simulations using the Ghost Fluid Method

Knut Sverdrup

*Cavendish Laboratory, Department of Physics, J J Thomson Avenue, Cambridge. CB3 0HE*

**Abstract**

The unsteady, compressible Euler equations for multimaterial flow in one dimension have been solved numerically by employing a level set method and two versions of the Ghost Fluid Method.

## 1. Introduction

Leonhard Euler first presented the momentum and continuity equations in 1757[1], which were completed by the adiabatic condition presented by Laplace in 1816[2]. The energy balance equation, which is the last of what is now called the Euler equations, was not properly incorporated until the late nineteenth century[3], and although the much more general Navier-Stokes equations have been developed[4,5], the continued interest for and usefulness of the Euler equations is undisputable. They provide a robust framework for analyzing ideal fluids when viscous effects are negligible, but cannot generally be solved analytically. Applications of the Euler equations include aerodynamics[6–8], atmospheric modelling and weather forecasts[9,10], astrophysics[11] and detonations and explosives[12–14], to name a few. Accordingly, precise and efficient methods for solving these non-linear, hyperbolic partial differential equations on arbitrary domains has been, and still is, a major field in modern computational fluid dynamics.

The Euler equations govern adiabatic and inviscid flow of a fluid. In the Froude limit (no external body forces) in one dimension, with density $\rho$, velocity $u$, total energy $E$ and pressure $p$, they are given by

$$\partial_t \mathbf{U} + \partial_x \mathbf{F}(\mathbf{U}) = 0 \,, \tag{1}$$

where the vector of conserved quantities $\mathbf{U}$ and their fluxes $\mathbf{F}(\mathbf{U})$ are given by

$$\mathbf{U} = \begin{bmatrix} \rho \\ \rho u \\ E \end{bmatrix} \,, \quad \mathbf{F} = \begin{bmatrix} \rho u \\ \rho u^2 + p \\ u(E + p) \end{bmatrix} \,.$$

It is sometimes convenient to work in terms of the primitive variables $\mathbf{W} = \begin{pmatrix} \rho, & u, & p \end{pmatrix}^T$. The total energy is the sum of the kinetic and potential energy of the system, i.e.

$$E = \frac{1}{2}\rho u^2 + \rho e \,, \tag{2}$$

where $e$ is the internal energy, related to the other variables through the equation of state. For an ideal gas, the equation of state is

$$e = \frac{p}{(\gamma - 1)\rho} \,, \tag{3}$$

where $\gamma$ denotes the ratio of specific heats for the gas. Several other fluids can be approximated by a so-called stiffened ideal gas equation of state,

$$e = \frac{p + \gamma p_\infty}{(\gamma - 1)\rho} \,. \tag{4}$$

Here, a material-dependent stiffening parameter $p_\infty$ has been introduced. Note that Eq. (4) reduces to Eq. (3) for materials with $p_\infty = 0$.

Many important milestones have led us to the current state of the art of solving the Euler equations numerically. Riemann identified and worked on the initial value problem for Eq. (1) with discontinuous initial conditions as early as 1860[15], but the first exact solution did not arrive until Godunov proposed an iterative scheme a century later[16]. Today, efficient approximate solvers such as HLLC (Harten-Lax-van Leer-Contact)[17] and Rotated-hybrid Riemann solvers[18] are readily available. The development of numerical analysis methods for partial differential equations got its first proper boost after the famous paper by Courant, Friedrichs and Lewis[19], but local Riemann problems[16], conservative methods[20] and finite volume formulations[21] were necessary before the first proper, three-dimensional simulations of the Euler equations could be performed in

the 1980s[22]. After the Monotonic Upstream-centered Scheme for Conservation Laws (MUSCL)[23] was introduced by van Leer as the first higher-order Total Variation Diminishing (TVD) scheme in 1979, several others have been developed, notably Toro's Weighted Average Flux (WAF)[24] and Flux/Slope LImiter Centred (SLIC/FLIC)[25] schemes.

Considerations of multimaterial interactions and flow are among the more recent (less than twenty year old) developments within numerical solutions for the Euler equations. It is the goal of this report to demonstrate some techniques available for multimaterial simulations of the Euler equations in one dimension. Different fluids are characterized by their material properties, such as $\gamma$, and thus special care must be taken in the treatment of boundaries separating different fluids.

Firstly, the location of the boundary must be tracked as time evolves. The most common way of doing this is by the use of level set methods, as proposed by Osher and Sethian[26]. The level set function for a region is initiated such that it is negative inside the region, positive outside it and zero on the boundary. By taking into consideration the convection of the fluids under consideration, the level set function is then evolved so that its zeros move with the domain boundary. Osher and Fedkiw[27] provide an excellent overview of level set methods and their applications.

Secondly, the interaction between different fluids across the material interfaces must be modelled accurately. In order to do so, Fedkiw *et al.* developed the Original Ghost Fluid Method (OGFM)[28]. In ghost fluid methods, each material has ghost cells on the side of the boundary where the other material exists. In the OGFM, the pressures and velocities at these ghost cells are similar to that of the other material, and the densities are calculated by enforcing constant entropy across the interface. This worked well for cases except when there were strong shock waves, since the entropy condition does not apply. As a response, the Modified Ghost Fluid Method (MGFM) was developed[29,30]. It is based on the realization that Riemann problems do not in general require the states on each side of the discontinuity to correspond to the same material. The cells in the ghost fluid are therefore updated by solving a local Riemann problem. A further development is the real Ghost Fluid Method (rGFM)[31], in which a more accurate interfacial boundary condition is applied. The implementation of the rGFM is outside the scope of this report.

The numerical methods which have been employed are explained in section 2, before several test cases and their results are discussed in section 3. Section 4 concludes the report.

## 2. Numerical methods

### 2.1. Riemann solvers

Given a conservation equation and two sets of piecewise constant states separated by a single discontinuity, the initial value problem of evolving this system in time is called a Riemann problem. It is very useful in the study of the Euler equations for two reasons. Firstly, it allows for exact (up to an arbitrary accuracy) solutions for systems obeying Eq. (1) which have a single contact discontinuity. The other benefit of Riemann solvers is that the discretization of space which is inevitable in computational schemes for solving differential equations, allows for precise solvers of conservation equations based on the solutions of many local Riemann problems.

For the Euler equations and initial conditions

$$\mathbf{W}(x, t = 0) = \begin{cases} \mathbf{W}_L, & x \le 0 \\ \mathbf{W}_R, & x > 0 \end{cases},$$

typical states the system can have are shown in Figure 1, in addition to characteristics for waves propagating in space-time. There are two types of resultant waves that propagate through space, in addition to the contact wave (dashed). The first is a shock wave, depicted as a thick line on the left, while the second is a rarefaction wave, shown as several gradually decaying lines on the right. Four different combinations of shock and rarefaction waves can occur on the left and right sides of the contact discontinuity, and the result is only dependent on $\mathbf{W}(x, 0)$.
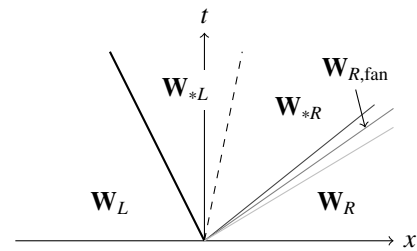


Figure 1: Possible wave configurations for the Riemann problem for Euler's equations in one dimension.

As seen from Figure 1, there are (up to) four unknown states for the Riemann problem: the left and right star states $\mathbf{W}_{*K}$ located between the left and right waves, and additionally the states inside rarefaction waves $\mathbf{W}_{K,\text{fan}}$. Note that the density in the $K$ star state depends on whether the corresponding wave is of shock of rarefaction type. One must therefore be able to compute all

these states, and also determine which of them is the correct one based on the speeds of the waves.

### 2.1.1. Exact solver

The exact solver, as first introduced by Godunov[16], has been implemented following Chapter 4 of Toro's comprehensive overview of Riemann solvers and their uses[32], but extended to take into consideration that different (stiffened) ideal gases may be present on each side of the discontinuity.

It can be proven that the pressure in the star states $p_*$ is given by the root of the nonlinear function

$$f(p) = f_L(p) + f_R(p) - (u_L - u_R).\qquad(5)$$

Here,

$$f_K(p) = \begin{cases} \frac{2a_K}{\gamma_K-1}\left[\left(\frac{p+p_{\infty,K}}{p_K+p_{\infty,K}}\right)^{\frac{\gamma_K-1}{2\gamma_K}} - 1\right], & p \le p_K \\ (p - p_K)\left(\frac{A_K}{B_K+p}\right)^{\frac{1}{2}}, & p > p_K \end{cases},$$

where $a_K = \sqrt{\frac{\gamma(p_K+p_{\infty,K})}{\rho_K}}$ is the speed of sound and

$$A_K = \frac{2}{(\gamma_K+1)\rho_K}, \qquad B_K = \frac{(\gamma_K-1)p_K + 2\gamma_K p_{\infty,K}}{\gamma_K+1}.$$

In the exact solver, the pressure in the star region is found by applying an iterative scheme to Eq. (5). Due to the nature of $f(p)$, it is well-suited for iterative schemes, but it is important to ensure that the pressure stays positive. For this project, Newton-Raphson iterations were implemented, taking the initial guess as $\frac{1}{2}(p_L + p_R)$. After finding $p_*$, the velocity in the star region is computed as

$$u_* = \frac{u_L + u_R - [f_L(p_*) - f_R(p_*)]}{2}.\qquad(6)$$

When the pressure and velocity in the star region have been computed, one can calculate the wave speeds (one per shock wave, two per rarefaction wave and one for the contact discontinuity) and use this to sample the state at a given point $S = x/t$ in space-time. Pseudocode for this procedure is given in Algorithm 1. Formulas for wave speeds and densities in different states have been left out for brevity, but they in general depend on the initial conditions (including material properties).

### 2.1.2. HLLC

By far the most computationally expensive part of the exact solver is the iterative root finding procedure for

**Data**: $S$, $\mathbf{W}_L$, $\mathbf{W}_R$, $p_*$, $u_*$, material properties
**Result**: $\mathbf{W}(S)$
**if** $S \le$ speed of contact discontinuity **then**
    **if** left wave is rarefaction **then**
        **if** $S \le$ speed of rarefaction head **then**
            return $\mathbf{W}_L$;
        **else**
            **if** $S >$ speed of rarefaction tail **then**
                return $\mathbf{W}_{*L,\text{fan}}$;
            **else**
                return $\mathbf{W}_{L,\text{fan}}$;
            **end**
        **end**
    **else**
        **if** $S \le$ speed of shock wave **then**
            return $\mathbf{W}_L$;
        **else**
            return $\mathbf{W}_{*L}$;
        **end**
    **end**
**else**
    perform similar analysis for sampling point on right side of contact discontinuity;
**end**

**Algorithm 1:** Sample exact solution of Riemann problem given pressure and velocity in star states.

finding $p_*$. Since most modern schemes require the solutions of local Riemann problems between all points in the computational domain, high gains in terms of computational efficiency can be achieved by employing exact solvers instead. One such solver is the Harten-Lax-van Leer-Contact (HLLC) solver, which has been implemented for this project.

When compared to the exact solver, the main simplifications in HLLC are that the pressure in the star region is approximated instead of found by iterative schemes; that states inside rarefactions are not taken into consideration, and that wave speeds are estimations, either direct or pressure-based. In this contribution, the pressure is estimated as

$$p_* \approx \frac{1}{2}(p_L + p_R) + \frac{1}{8}(u_L - u_R)(\rho_L + \rho_R)(a_L + a_R),\ (7)$$

and set equal to zero if the approximation is negative. Based on the approximation for $p_*$, the wave speeds $S_K$ of the left and right travelling waves are computed, with the type of wave taken into consideration. The speed of the contact discontinuity is then approximated as

$$S_* \approx \frac{\rho_L u_L (S_L - u_L) - \rho_R u_R (S_R - u_R) - (p_L - p_R)}{\rho_L (S_L - u_L) - \rho_R (S_R - u_R)}.$$
(8)

There are four possible states, separated by the three (approximated) wave speeds. Contrary to the exact solver, where the output is the state $\mathbf{W}(S)$, the HLLC solver outputs a flux $\mathbf{F}^{\text{HLLC}}$ based on the state corresponding to $S = 0$. This is because the flux at the intermediate point between cells is the quantity employed in the update formula as introduced in Subsection 2.2. For an overview of the approximate states and the flux calculation employed in the HLLC solver, see Chapter 9 of Toro's book[32].

### 2.2. Schemes for the Euler equations

When the Euler equations are given as in Eq. (1), they are said to be a system of conservation equations in differential form. In integral form, on a spatial domain $[x_L, x_R]$, the same system of equations can be written

$$\int_{x_L}^{x_R} \mathbf{U}(x, t_2) \mathrm{d}x = \int_{x_L}^{x_R} \mathbf{U}(x, t_1) \mathrm{d}x - \int_{t_1}^{t_2} \mathbf{F}(\mathbf{U}(x_R, t)) \mathrm{d}x$$
$$+ \int_{t_1}^{t_2} \mathbf{F}(\mathbf{U}(x_L, t)) \mathrm{d}x.$$
(9)

Explain fintite volume, conservative schemes and the difference between centered and RP-based schemes.

#### 2.2.1. MUSCL-Hancock
#### 2.2.2. SLIC
### 2.3. Level-set method
### 2.4. Ghost Fluid Methods
#### 2.4.1. Original Ghost Fluid Method
#### 2.4.2. Modified Ghost Fluid Method
## 3. Results

### 3.1. Moving contact discontinuity

### 3.2. Simple ghost fluid tests

### 3.3. Multimaterial shock tubes for gases

### 3.4. Water-gas shock tube test

## 4. Conclusions

Everythings went better as expectance!

[1] L. Euler, Principes généraux de l'état d'équilibre d'un fluide, Académie Royale des Sciences et des Belles Lettres de Berlin 11 (1757) 217–273.

[2] P.-S. de Laplace, Sur la vitesse du son dans l'air et dans l'eau, Annales de Chimie et de Physique 3 (1816) 283–241.

[3] D. Christodoulou, The Euler equations of compressible fluid flow, Bulletin of the American Mathematical Society 44 (4) (2007) 581–602.

[4] C. L. M. H. Navier, Memoire sur les lois du mouvement des fluides, Mémoires de l'Académie Royale des Sciences de l'Institut de France 6 (1822) 389–440.

[5] G. G. Stokes, On the theories of the internal friction of fluids in motion and of the equilibrium and motion of elastic solids, Transactions of the Cambridge Philosophical Society 8 (1845) 287–319.

[6] M. Drela, Two-dimensional transonic aerodynamic design and analysis using the Euler equations, Ph.D. thesis, Massachusetts Institute of Technology (1985).

[7] W. K. Anderson, J. L. Thomas, B. Van Leer, Comparison of finite volume flux vector splittings for the Euler equations, AIAA journal 24 (9) (1986) 1453–1460.

[8] G. P. Guruswamy, Unsteady aerodynamic and aeroelastic calculations for wings using Euler equations, AIAA journal 28 (3) (1990) 461–469.

[9] R. Laprise, The Euler equations of motion with hydrostatic pressure as an independent variable, Monthly weather review 120 (1) (1992) 197–207.

[10] W. C. Skamarock, J. B. Klemp, A time-split nonhydrostatic atmospheric model for weather research and forecasting applications, Journal of Computational Physics 227 (7) (2008) 3465–3485.

[11] H. Trac, U.-L. Pen, A primer on Eulerian computational fluid dynamics for astrophysics, Publications of the Astronomical Society of the Pacific 115 (805) (2003) 303.

[12] N. Nikiforakis, J. Clarke, Numerical studies of the evolution of detonations, Mathematical and Computer Modelling 24 (8) (1996) 149–164.

[13] D. N. Williams, L. Bauwens, E. S. Oran, Detailed structure and propagation of three-dimensional detonations, in: Symposium (International) on Combustion, Vol. 26, Elsevier, 1996, pp. 2991–2998.

[14] R. Saurel, O. Lemetayer, A multiphase model for compressible flows with interfaces, shocks, detonation waves and cavitation, Journal of Fluid Mechanics 431 (2001) 239–271.

[15] B. Riemann, Über die Fortpflanzung ebener Luftwellen von endlicher Schwingungsweite, Verlag der Dieterichschen Buchhandlung, 1860.

[16] S. K. Godunov, A difference method for numerical calculation of discontinuous solutions of the equations of hydrodynamics, Matematicheskii Sbornik 89 (3) (1959) 271–306.

[17] E. F. Toro, M. Spruce, W. Speares, Restoration of the contact surface in the HLL-Riemann solver, Shock Waves 4 (1) (1994) 25–34.

[18] H. Nishikawa, K. Kitamura, Very simple, carbuncle-free, boundary-layer-resolving, rotated-hybrid Riemann solvers, Journal of Computational Physics 227 (4) (2008) 2560–2581.

[19] R. Courant, K. Friedrichs, H. Lewy, Über die partiellen Differenzengleichungen der mathematischen Physik, Mathematische Annalen 100 (1) (1928) 32–74.

[20] P. Lax, B. Wendroff, Systems of conservation laws, Communications on Pure and Applied mathematics 13 (2) (1960) 217–237.
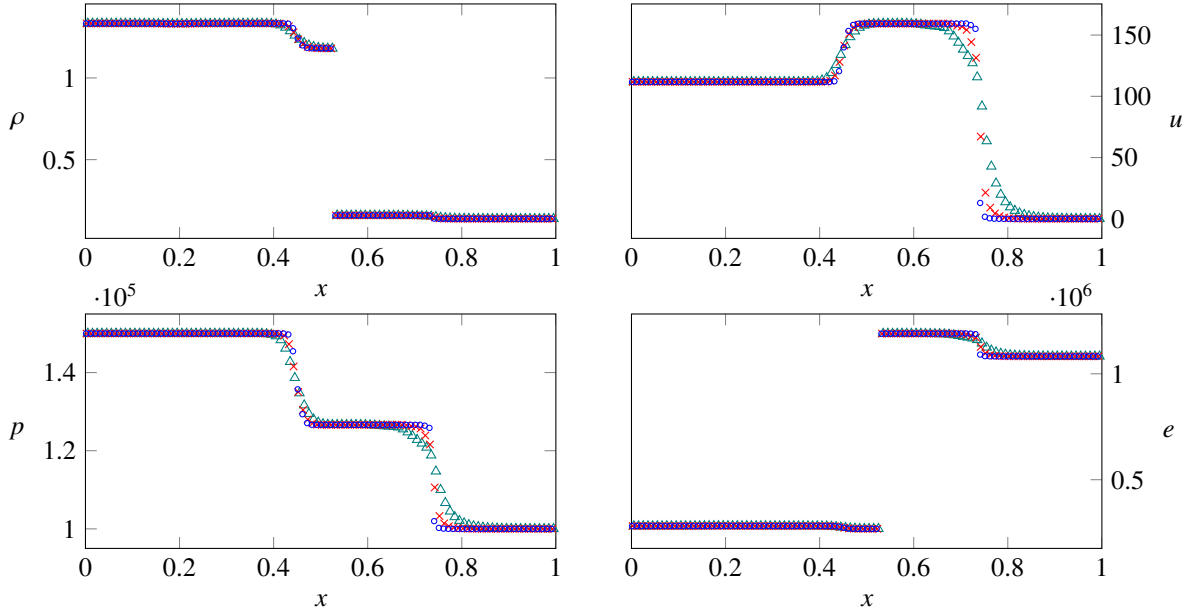
Figure 2: Original Ghost Fluid method for test C. △$N = 100$ ×$N = 200$ ○$N = 400$

[21] R. J. LeVeque, Finite volume methods for hyperbolic problems, Vol. 31, Cambridge university press, 2002.

[22] A. Jameson, W. Schmidt, E. Turkel, et al., Numerical solutions of the Euler equations by finite volume methods using Runge-Kutta time-stepping schemes, AIAA paper 1259.

[23] B. van Leer, Towards the ultimate conservative difference scheme. V. A second-order sequel to Godunov's method, Journal of Computational Physics 32 (1) (1979) 101–136.

[24] E. Toro, A weighted average flux method for hyperbolic conservation laws, in: Proceedings of the Royal Society of London A: Mathematical, Physical and Engineering Sciences, Vol. 423, The Royal Society, 1989, pp. 401–418.

[25] E. Toro, S. Billett, Centred TVD schemes for hyperbolic conservation laws, IMA Journal of Numerical Analysis 20 (1) (2000) 47–79.

[26] S. Osher, J. A. Sethian, Fronts propagating with curvature-dependent speed: algorithms based on Hamilton-Jacobi formulations, Journal of Computational Physics 79 (1) (1988) 12–49.

[27] S. Osher, R. P. Fedkiw, Level set methods: an overview and some recent results, Journal of Computational physics 169 (2) (2001) 463–502.

[28] R. P. Fedkiw, T. Aslam, B. Merriman, S. Osher, A non-oscillatory Eulerian approach to interfaces in multimaterial flows (the ghost fluid method), Journal of Computational Physics 152 (2) (1999) 457–492.

[29] T. Liu, B. Khoo, K. Yeo, Ghost fluid method for strong shock impacting on material interface, Journal of Computational Physics 190 (2) (2003) 651–681.

[30] S. K. Sambasivan, H. Udaykumar, Ghost fluid method for strong shock interactions part 1: Fluid-fluid interfaces, AIAA Journal 47 (12) (2009) 2907–2922.

[31] C. Wang, T. Liu, B. Khoo, A real ghost fluid method for the simulation of multimedium compressible flow, SIAM Journal on Scientific Computing 28 (1) (2006) 278–302.

[32] E. F. Toro, Riemann solvers and numerical methods for fluid dynamics: a practical introduction, Springer Science & Business Media, 2013.
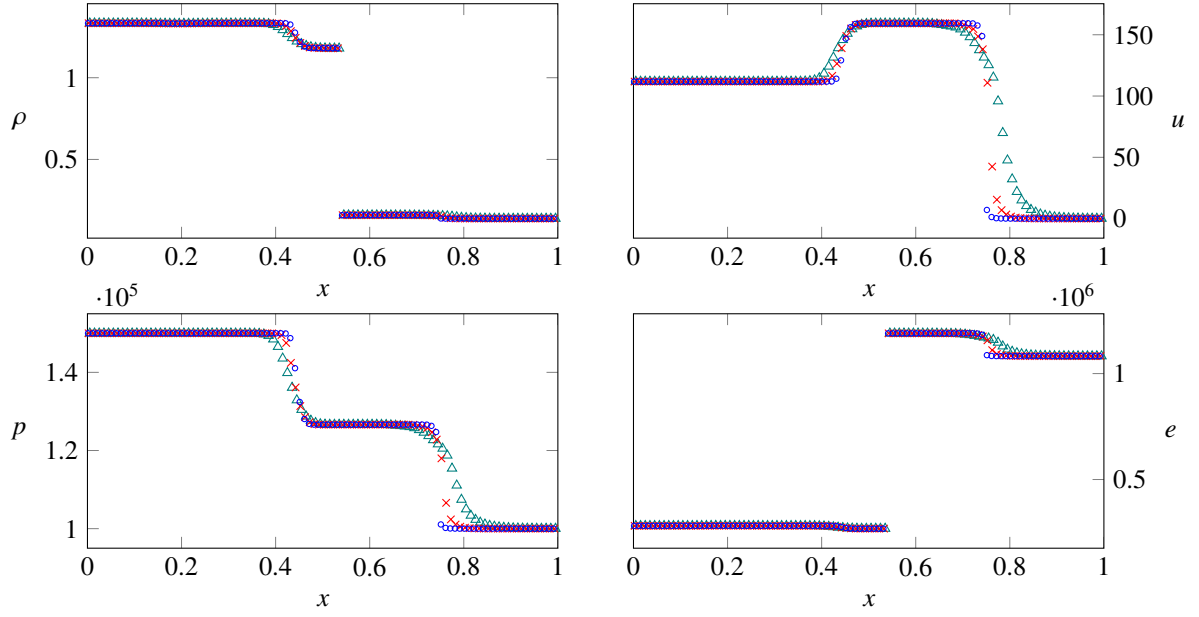
Figure 3: Riemann Ghost Fluid method for test C. △$N = 100$ ×$N = 200$ ○$N = 400$
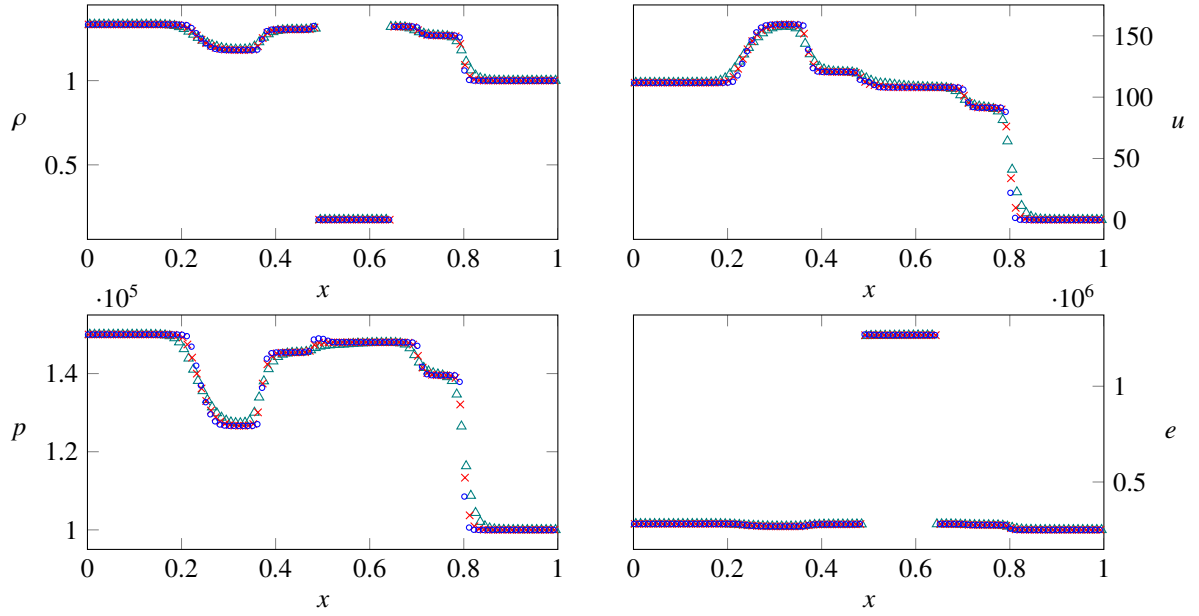


Figure 4: Original Ghost Fluid method for test D. △$N = 100$ ×$N = 200$ ○$N = 400$
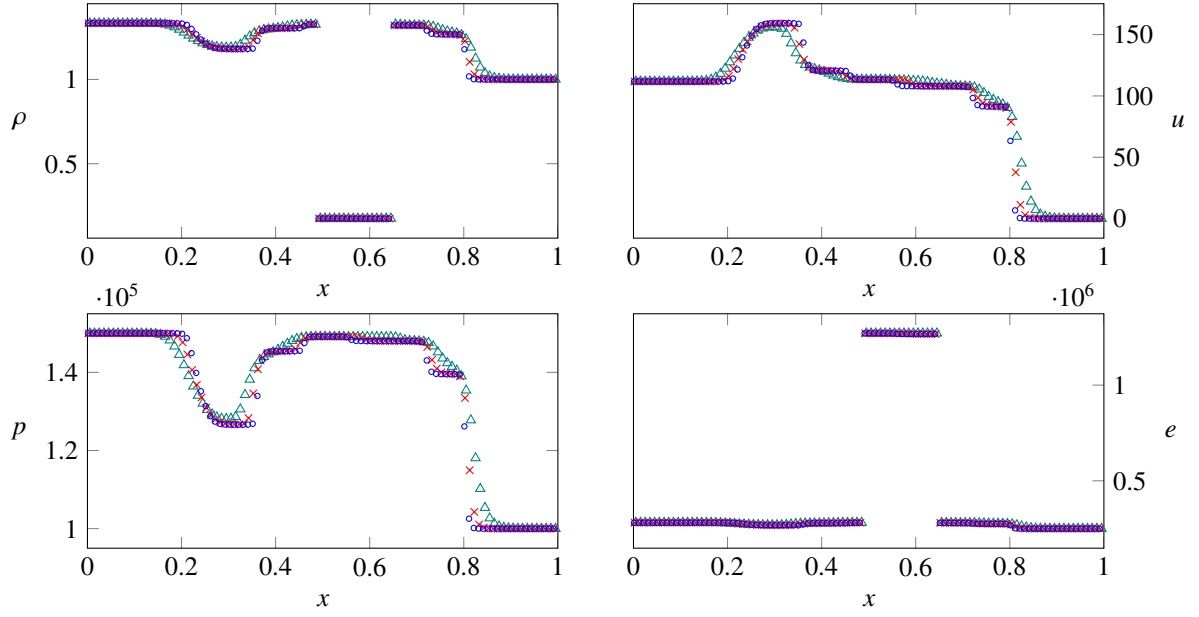
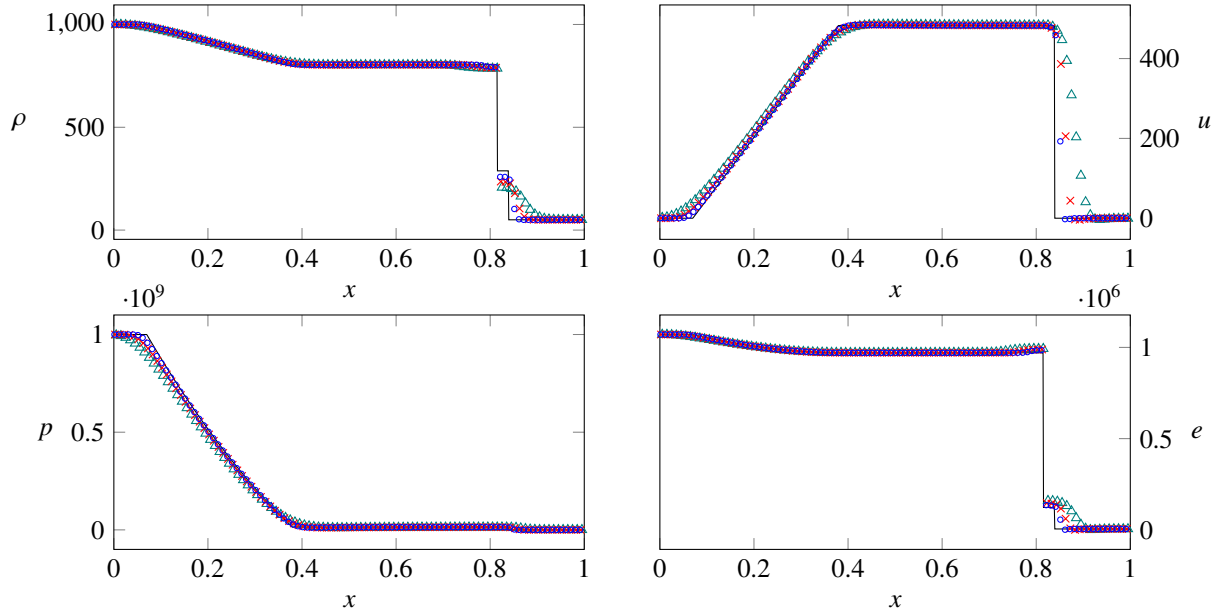Figure 5: Riemann Ghost Fluid method for test D. △$N = 100$ ✕$N = 200$ ○$N = 400$



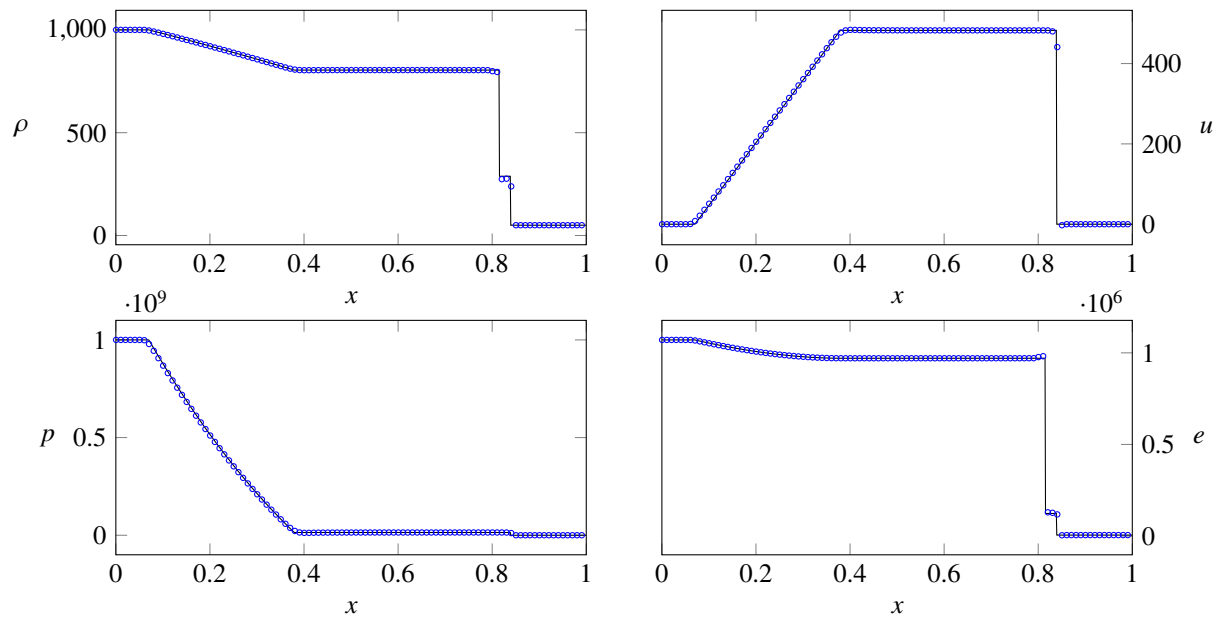Figure 6: Riemann Ghost Fluid method for test E. △$N = 100$ ✕$N = 200$ ○$N = 400$

Figure 7: Riemann Ghost Fluid method for test E with higher accuracy ($N = 1000$).